Statistical mechanics of the Euler-equations without vortex stretching

Tong Wu, Wouter J T Bos

Statistical mechanics of the Euler-equations without vortex stretching

Tong Wu and Wouter J. T. Bos†

Univ Lyon, CNRS, Ecole Centrale de Lyon, INSA Lyon, Univ Claude Bernard Lyon 1, LMFA, UMR5509, 69340 Ecully, France

(Received 2021)

We consider the relaxation to thermal equilibrium of the Galerkin-truncated Euler-equations in three-dimensions, from which vortex-stretching is removed. We prove that helicity and enstrophy are conserved by the system. Using statistical mechanics, we derive analytical predictions for the equilibrium energy and helicity spectra. Results are verified using pseudo-spectral direct numerical simulations. Results show that if the initial condition contains helicity, the system relaxes to a force-free large-scale structure akin to an ABC flow.

1. Introduction

The dynamics of two and three-dimensional turbulence are dramatically different. Whereas in three dimensions kinetic energy shows the tendency to cascade towards the small-scales (Kolmogorov 1941), in two dimensions energy is more inclined to concentrate in space-filling vortical structures (Kraichnan 1967; Onsager 1949). A question that we have addressed recently (Bos 2021), is whether this difference in behavior is a direct consequence of the change in dimension, or that it is caused by the geometrical fact that in two-dimensional flows the velocity-gradient is perpendicular to the vorticity, which removes the vortex-stretching from the dynamics. In the framework of the Navier-Stokes equations, these two possibilities seem equivalent, since the change from three to two dimensions leads to the suppression of vortex-stretching. However, it is possible to formulate a three-dimensional variant of the Navier-Stokes equations, where vortex-stetching is removed in every point in space. One way to interpret this system is that we consider two-dimensional three-component dynamics in an isotropic three-dimensional setting, another is that we apply a force to the three-dimensional Navier-Stokes equations, which compensates for the vortex-stretching term.

Either way, this turbulence without vortex-stretching, in the absence of forces and viscosity, reduces the dynamics to a flow governed by the modified Euler-equation,

$$\frac{\partial \boldsymbol{\omega}}{\partial t} + \boldsymbol{u} \cdot \nabla \boldsymbol{\omega} = 0, \tag{1.1}$$

with $\boldsymbol{\omega} = \nabla \times \boldsymbol{u}$ and $\boldsymbol{u}$ the velocity. In Bos (2021) we showed using closure analysis that turbulence without vortex-stretching, which conserves enstrophy defined as

$$W = \frac{1}{2}\langle \boldsymbol{\omega} \cdot \boldsymbol{\omega} \rangle \tag{1.2}$$

† Email address for correspondence: wouter.bos@ec-lyon.fr

with $\langle \bullet \rangle$ a volume average, shows a tendency to cascade this enstrophy to the small scales of the system as in two-dimensional turbulence (Batchelor 1969; Leith 1968; Kraichnan 1967). In that work we did not observe conservation of any other quantity by the system. Indeed, kinetic energy,

$$E = \frac{1}{2}\langle \boldsymbol{u} \cdot \boldsymbol{u} \rangle, \tag{1.3}$$

is not conserved by three dimensional turbulence without vortex-stretching. We considered however the specific case of mirror-symmetry, i.e., a flow without mean-helicity. In the present investigation we proof first that helicity is conserved by the system. Then, using statistical mechanics and numerical simulations, we show that the presence of helicity completely changes the dynamics of the system. We note here that our manner of removing the vortex-stretching also removes strain-self-amplification (Carbone & Bragg 2020; Johnson 2020) and simultaneously removes both local and nonlocal contributions to the strain induced by vortex-stretching (Buaria *et al.* 2020).

One might obviously question the relevance of turbulence without vortex-stretching to realistic turbulent flows. We have discussed this to some extent in Bos (2021). Reasons to further investigate this system are actually numerous. A first justification is, as in Bos (2021), to better understand the role of vortex-stretching by removing it. Indeed, recently an important body of research has focused on the decimation of turbulence to investigate its dynamics (Frisch *et al.* 2012; Biferale *et al.* 2012; Alexakis 2017). Also Kraichnan's test-field model (Kraichnan 1971) is based on the removal of a particular feature of the turbulent dynamics, the incompressibility constraint, to measure the Lagrangian decorrelation induced by pressure fluctuations. Yet another important motivation to study the present system is mathematical, since the main difficulty in the mathematical study of the singularity of the incompressible 3D Euler equations is the stretching and amplification of vorticity (Constantin 2007; Kerr 1993; Hou & Li 2006). The removal of the vortex-stretching term might give a handle on this challenging problem. For instance, in future investigation, the vortex stretching can be introduced only partially, or locally, to assess how strong vortex stretching must be for singular structures to be created. A motivation which was not so clearly mentioned before, is the following. Two-dimensional three-component flows are important asymptotic states in turbulence (Biferale *et al.* 2017). For instance, we can mention rapidly rotating turbulence or turbulence in the presence of a magnetic field (Davidson 2013; Sagaut & Cambon 2008). The present turbulent flow is in some sense the three-dimensional isotropic analog of such flows. We think that the present isotropic case, which is geometrically rather simple to describe, shares certain key features with 2D3C flows, such as the conservation of helicity. In order for the present flow to be valuable in these above mentioned applications, we should understand its main features.

In the next section we will briefly recall the relevance of statistical mechanics to turbulence research. Then, in section 3 we will show that helicity and enstrophy are conserved by the modified Euler-equation. Subsequently we will derive the statistical mechanics equilibrium predictions for the energy spectrum. The shape of the resulting equilibrium spectrum suggests that in the absence of vortex-stretching, helicity might play an important role in the dynamics of turbulence, unlike the classical three-dimensional case. Sec. 4 presents the numerical method and the generation of initial conditions. In Sec. 5 we present a numerical assessment of the theoretical results, including analyses of the conserved quantities, equilibrium spectra, and the physical-space characterization of the velocity field. Sec. 6 presents the conclusions.

2. Equilibrium statistical mechanics of the Euler-equations

The study of turbulence using equilibrium statistical mechanics started with the work of Onsager (1949). Not so long after that, Lee (1952) showed that if the Galerkin-truncated Euler equations are analyzed, a Liouville equation can be formulated which allows a direct application of equilibrium statistical mechanics. The reasoning, which we will discuss in more detail in this investigation, is that if the Euler-equations are represented by a finite number of Fourier modes, their dynamics is incompressible in phase-space. Applying then equilibrium statistical mechanics to the Fourier-modes leads to the prediction of the most probable, thermal-equilibrium state, corresponding to an equidistribution of energy over all accessible locations of phase-space. The Fourier-distribution of kinetic energy is given by

$$U(k) = \frac{1}{2}\langle \boldsymbol{u}(\boldsymbol{k}) \cdot \boldsymbol{u}^*(\boldsymbol{k}) \rangle \tag{2.1}$$

with $\boldsymbol{u}(\boldsymbol{k})$ the Fourier-coefficient associated with the velocity at wavevector $\boldsymbol{k}$ and k the norm of this wavevector. Lee's result implies that the average energy distribution is simply constant

$$U(k) = \text{constant} = 2/\alpha, \tag{2.2}$$

where the constant is named $2/\alpha$, for later convenience. This energy-distribution corresponds to an isotropic kinetic energy spectrum,

$$E(k) = 4\pi k^2 U(k) = \frac{8\pi k^2}{\alpha}. \tag{2.3}$$

We note that the energy spectrum is here and in the following distinguished from the kinetic energy by its argument k. Expression (2.3) is radically different from observations of freely evolving three-dimensional Navier-Stokes turbulence, which displays a close to $k^{-5/3}$ wavenumber dependence over a wide range of scales. However, it can be concluded from this analysis that turbulence with kinetic energy at large scales will have a tendency to transfer turbulent excitation towards the smaller scales as to approach this equilibrium state. Indeed, since the large scales (small k) of high-Reynolds numbers turbulence are nearly unaffected by viscous-stresses, these scales are approximately obeying the Euler equations. For instance, in forced three-dimensional turbulence, an energy spectrum close to expression (2.3) is observed (Lesieur 1990; Alexakis & Brachet 2019) for wavenumbers k smaller than the wavenumber associated with the forcing. If we let these large scales freely evolve, the tendency of the large scales, piloted by the Euler-equations will transfer energy to larger k. In natural systems, viscous dissipation will damp this energy if the wavenumber is large enough so that the equilibrium state (2.3) is never attained in the absence of external forcing. Equilibrium statistical mechanics do therefore help to determine cascade directions.

The analysis by Lee considered the kinetic energy of the three-dimensional turbulent fluctuations as the only invariant of the system. In the 1960s another invariant was shown to exist in three-dimensional bounded flow (Moreau 1961; Moffatt 1969). This invariant is named helicity and is defined as

$$H = \frac{1}{2}\langle \boldsymbol{u} \cdot \boldsymbol{\omega} \rangle. \tag{2.4}$$

After the introduction of the concept of helicity, it was anticipated by Kraichnan (1973) using equilibrium statistical mechanics that the presence of helicity should not dramatically influence the dynamics. The principal reasoning to come to this insight was based on an analysis similar to that of Lee. The equilibrium state he derived for the kinetic energy

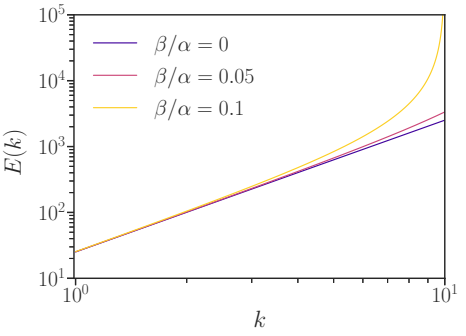

Figure 1: Absolute equilibrium energy spectra for three-dimensional turbulence with and without helicity.

spectrum is

$$E(k) = \frac{8\pi\alpha k^2}{\alpha^2 - \beta^2 k^2}, \tag{2.5}$$

where β is a Lagrange multiplier. This expression is sketched in Fig. 1. We show how the presence of helicity alters the equilibrium prediction (2.3) for the kinetic energy spectrum for three cases, with value $\beta = 0$, i.e., zero helicity, $\beta k_{\max}/\alpha = 1$, the maximum helical case, and an intermediate case. Even for the most helical case, the large scales are unaffected and only the highest wavenumbers display the influence of the helicity on the energy distribution. Again, these scales are in real turbulence damped by viscous dissipation. From this analysis Kraichnan concluded that the influence of helicity on three-dimensional turbulence should be small. This was confirmed soon after using two-point closure (André & Lesieur 1977), and later by direct numerical simulations (Borue & Orszag 1997).

A situation where the presence of two distinct invariants does change the dynamics considerably is the case of two-dimensional turbulence. In such flows, the enstrophy is conserved together with the energy. For this case, Kraichnan (1967) derived equilibrium predictions and deduced the directions of energy and enstrophy cascades.

Since these pioneering investigations, a wide range of turbulent systems have been analyzed using statistical mechanics. The most well-known approaches are the equilibrium states computed using a point-vortex approach of 2D turbulence (Onsager 1949; Montgomery & Joyce 1974; Lundgren & Pointin 1977) and the equilibrium theory of Robert & Sommeria (1991) and Miller (1990), considering coarse-grained 2D turbulence (see also Eyink & Spohn (1993)). A large variety of problems has since then been tackled using statistical mechanics such as the prediction of mixing in stratified turbulence (Venaille *et al.* 2017), vorticity in a vortex-ring (Mohseni 2001), axisymmetric turbulence as applied to Von-Karman flow (Leprovost *et al.* 2006; Naso *et al.* 2010), the characterization of magnetohydrodynamic turbulence (Frisch *et al.* 1975; Fyfe & Montgomery 1976; Servidio *et al.* 2008), of plasma turbulence (Zhu & Hammett 2010) and random reversals in turbulent systems Shukla *et al.* (2016). An investigation, somewhat similar to the present one, gives insights in the coupling of different two-dimensional turbulent velocity fields (Salmon 2013). In a recent manuscript (van Kan *et al.* 2021) further motivations are given to study truncated turbulent systems using statistical mechanics.

A complete review is beyond the scope of the present investigation. Therefore we refer for extensive reviews on statistical mechanics applied to two-dimensional turbulence to

Kraichnan & Montgomery (1980) for the older work and to Bouchet & Venaille (2012) for more recent developments.

3. Analytical considerations

In this section we will first prove that the nonlinearity of the vorticity-advection equation conserves both enstrophy and helicity. Using this information, we then formulate a statistical mechanics of the truncated system. The presence of the two invariant quantities (enstrophy and helicity) leads, for non-zero helicity, to a thermal equilibrium state with energy peaking at the largest possible scale of the system. This conclusion is opposite to the result for classic three-dimensional turbulence, where helicity only modifies the smallest alowed scales of the system, as was observed in Fig. 1.

3.1. *Conservation of integral quantities*

The governing equation of our system is Eq. (1.1). Multiplying by $\boldsymbol{\omega}$ and averaging yields

$$\frac{dW}{dt} = -\langle \boldsymbol{\omega} \cdot (\boldsymbol{u} \cdot \nabla \boldsymbol{\omega}) \rangle, \tag{3.1}$$

where $W = \frac{1}{2} \left\langle \|\boldsymbol{\omega}\|^2 \right\rangle$. Incompressibility allows to write

$$\frac{dW}{dt} = -\frac{1}{2} \nabla \cdot \langle \boldsymbol{u} \|\boldsymbol{\omega}\|^2 \rangle, \tag{3.2}$$

and the integral of the gradient-term on the right-hand side is zero for statistically homogeneous, or periodic, flows so that we obtain conservation of enstrophy,

$$\frac{dW}{dt} = 0. \tag{3.3}$$

The proof of conservation of helicity is somewhat more involved and follows the same reasoning as in Frisch (1995) for the Euler equations. We need the relations,

$$\langle f \nabla g \rangle = -\langle g \nabla f \rangle \tag{3.4}$$

$$\langle \boldsymbol{f} \cdot \nabla \times \boldsymbol{g} \rangle = \langle \boldsymbol{g} \cdot \nabla \times \boldsymbol{f} \rangle, \tag{3.5}$$

valid for arbitrary scalar fields f, g and vector fields $\boldsymbol{f}, \boldsymbol{g}$. Furthermore for incompressible fields $\boldsymbol{u}$, $\boldsymbol{\omega}$, we have

$$\nabla \times (\boldsymbol{u} \times \boldsymbol{\omega}) = \boldsymbol{\omega} \cdot \nabla \boldsymbol{u} - \boldsymbol{u} \cdot \nabla \boldsymbol{\omega}. \tag{3.6}$$

The proof of helicity conservation goes as follows. Helicity is defined as

$$H = \frac{1}{2} \langle \boldsymbol{\omega} \cdot \boldsymbol{u} \rangle. \tag{3.7}$$

The evolution of H is then given by

$$\frac{dH}{dt} = \frac{1}{2} \left(\left\langle \frac{\partial \boldsymbol{\omega}}{\partial t} \cdot \boldsymbol{u} \right\rangle + \left\langle \frac{\partial \boldsymbol{u}}{\partial t} \cdot \boldsymbol{\omega} \right\rangle \right) \tag{3.8}$$

which can be written using (3.5) as

$$\frac{dH}{dt} = \left\langle \frac{\partial \boldsymbol{\omega}}{\partial t} \cdot \boldsymbol{u} \right\rangle \tag{3.9}$$

which avoids the need to know the equation for $\partial \boldsymbol{u} / \partial t$. Using vector-identity Eq. (3.6), we

can rewrite the vorticity equation (3.1),

$$\frac{\partial \boldsymbol{\omega}}{\partial t} = \nabla \times (\boldsymbol{u} \times \boldsymbol{\omega}) - (\boldsymbol{\omega} \cdot \nabla)\boldsymbol{u}, \tag{3.10}$$

so that for the time-evolution of helicity we can write,

$$\frac{dH}{dt} = \langle \boldsymbol{u} \cdot \nabla \times (\boldsymbol{u} \times \boldsymbol{\omega}) \rangle - \langle \boldsymbol{u} \cdot (\boldsymbol{\omega} \cdot \nabla \boldsymbol{u}) \rangle \tag{3.11}$$

where both terms on the right-hand-side can be shown to be zero using expressions (3.4) and (3.5) and incompressibility. We note here that this proof can be extended to the case of two-dimensional three-component flows (Biferale *et al.* 2017).

We note that the conservation of helicity is a global flow property in our system. For the original Euler-equations, helicity is not only a global property, but is also conserved in sub-domains consisting of closed vortex-tubes. The proof of this requires that forces applied to the system are irrotational (Moffatt 1969). The system considered in the present investigation can be seen as the Euler equation to which we apply a force which compensates for vortex stretching in every point in space (Bos 2021). Since the curl of this force is equal to (minus) the vortex-stretching term in the vorticity equation, it is easily observed that this force is not irrotational, and helicity in the present system is therefore not conserved in closed vortex tubes.

Strictly spoken, the enstrophy and the helicity are not the only conserved quantities. Indeed, as for two-dimensional turbulence, all other even powers of the vorticity, $\langle \|\boldsymbol{\omega}\|^{2n} \rangle$ are conserved by the system. Furthermore, not only the total enstrophy is conserved, but also the individual components, $\langle \omega_x^2 \rangle$, $\langle \omega_y^2 \rangle$ and $\langle \omega_z^2 \rangle$ are conserved independently. We will consider the case where these different contributions are comparable, so that we can focus on the sum of the contributions, the total enstrophy.

3.2. *Statistical equilibrium distributions*

In this section we will derive, using tools from statistical mechanics, the spectral energy distribution corresponding to thermal equilibrium of a finite set of Fourier-modes. We refer to Salmon (1998) and Thalabard (2013) for detailed derivations using the present approach. We consider that the flow is decomposed on a finite number N of Fourier-components $\boldsymbol{u}(\boldsymbol{k})$. The vector-space $\boldsymbol{k}$ is thus decomposed by its coordinates $\boldsymbol{k}_n$, with $n = 1..N$. Note that in this section, the subscript n does not indicate a vector index, but simply a counter. The value N corresponds to the total number of modes. This means that in a three-dimensional cubic domain with N_{k_x} modes in each direction, $N = N_{k_x}^3$. Note that the Fourier coefficients of velocity satisfy the conjugate symmetry $\boldsymbol{u}(\boldsymbol{k}) = \boldsymbol{u}^*(-\boldsymbol{k})$, because the velocity is a real quantity in physical space, thus the total number of independent degrees of freedoms of the system is $N/2$.

We consider incompressible flow, where the divergence in Fourier-space implies $\boldsymbol{k} \cdot \boldsymbol{u}(\boldsymbol{k}) = 0$, so that only two-independent Fourier-coefficients are needed to represent the velocity-vector $\boldsymbol{u}(\boldsymbol{k}_n)$. Since, in addition, the Fourier-coefficients are complex, in total 4 independent real coefficients describe each mode. These modes are denoted $y_{n_1}, y_{n_2}, y_{n_3}, y_{n_4}$, where n runs from 1 to N. In total therefore, if we have N wave-vector coordinates representing a three-dimensional velocity field, we have to consider the dynamics of a system of $4N$ coordinates in phase-space. A convenient way to choose the independent modes will be described now.

Following Waleffe (1992), Cambon & Jacquin (1989) and Kraichnan (1973), we represent the velocity field of an incompressible 3D fluid by using a helical-mode decomposition. Every 3D Fourier vector $\boldsymbol{u}(\boldsymbol{k})$ can be represented by two orthogonal complex helical waves

$\boldsymbol{h}^{\pm} = \hat{\boldsymbol{w}} \times \hat{\boldsymbol{k}} \pm \mathrm{i}\hat{\boldsymbol{w}}$ with $\hat{\boldsymbol{k}} = \boldsymbol{k}/k$ the unit vector parallel to $\boldsymbol{k}$. Here the unit vector $\hat{\boldsymbol{w}}$ can be chosen as $\hat{\boldsymbol{w}} = \boldsymbol{z} \times \boldsymbol{k}/|\boldsymbol{z} \times \boldsymbol{k}|$ for an arbitrary vector $\boldsymbol{z}$. It then follows that

$$\boldsymbol{u}(\boldsymbol{k}) = u^{+}(\boldsymbol{k})\boldsymbol{h}^{+}(\boldsymbol{k}) + u^{-}(\boldsymbol{k})\boldsymbol{h}^{-}(\boldsymbol{k})\,. \tag{3.12}$$

Note that $u^{+}(\boldsymbol{k})$ and $u^{-}(\boldsymbol{k})$ are complex numbers.

As stated above, all coordinates $\boldsymbol{k}$ of the considered part of Fourier space are individually labeled $\boldsymbol{k}_n$, with n ranging from 1 to N. Since at each coordinate $\boldsymbol{k}_n$ we have 4 individual real coefficients $y_{n_1}, y_{n_2}, y_{n_3}, y_{n_4}$, we can thus define using this representation,

$$\begin{aligned} y_{n_1} &= \Re(u^{+}(\boldsymbol{k}_n)), \quad y_{n_2} = \Im(u^{+}(\boldsymbol{k}_n)), \\ y_{n_3} &= \Re(u^{-}(\boldsymbol{k}_n)), \quad y_{n_4} = \Im(u^{-}(\boldsymbol{k}_n)). \end{aligned} \tag{3.13}$$

The main motivation to use the helical mode decomposition in the present investigation is that we have a simple relation between the generalized coordinates and the modal energy, helicity and enstrophy,

$$\begin{aligned} \frac{1}{2}\boldsymbol{u}(\mathbf{k}) \cdot \boldsymbol{u}^{*}(\mathbf{k}) &= u_{+}u_{+}^{*} + u_{-}u_{-}^{*} \\ &= y_{n_1}^2 + y_{n_2}^2 + y_{n_3}^2 + y_{n_4}^2 = E_n, \end{aligned} \tag{3.14}$$

$$\begin{aligned} \frac{1}{2}\boldsymbol{u}(\mathbf{k}) \cdot \boldsymbol{\omega}^{*}(\mathbf{k}) &= k\left(u_{+}u_{+}^{*} - u_{-}u_{-}^{*}\right) \\ &= |\boldsymbol{k}_n|\left(y_{n_1}^2 + y_{n_2}^2 - y_{n_3}^2 - y_{n_4}^2\right) = H_n, \end{aligned} \tag{3.15}$$

$$\begin{aligned} \frac{1}{2}\boldsymbol{\omega}(\mathbf{k}) \cdot \boldsymbol{\omega}^{*}(\mathbf{k}) &= k^2(u_{+}u_{+}^{*} + u_{-}u_{-}^{*}) \\ &= |\boldsymbol{k}_n|^2(y_{n_1}^2 + y_{n_2}^2 + y_{n_3}^2 + y_{n_4}^2) = W_n. \end{aligned} \tag{3.16}$$

In the following we will use that all four coefficients y_n correspond to the same position in Fourier-space so that we can write $|\boldsymbol{k}_n| = k$. Now that we have defined the invariants as a function of the generalized coordinates y_{n_i} in phase space, we can proceed the derivation of the equilibrium distribution.

The fundamental principle of equilibrium statistical mechanics states that in systems satisfying a Liouville equation (nondivergent evolution of the generalized coordinates), the probability density $P(\mathbf{y})$ eventually becomes uniform over all accessible parts of phase space (Salmon 1998). We will compute the average spectral energy distribution associated with this thermal equilibrium state. An essential ingredient to compute the average corresponding to this distribution is the probability density. The partial density, or partition function for mode n, $P_n\left(y_{n_1}, ..., y_{n_4}\right)$ is considered to satisfy a Boltzmann-Gibbs equilibrium distribution,

$$P_n\left(y_{n_1}, ..., y_{n_4}\right) = C_n \exp\left[-S_n\right] \tag{3.17}$$

where S_n is a function of the constants of motion and C_n is a constant. For instance, if enstrophy and helicity are conserved, as in our case, the quantity S_n writes

$$S_n = \alpha W_n + \beta H_n, \tag{3.18}$$

where α and β are Lagrange multipliers representing some kind of inverse statistical temperature or chemical potential. The function P_n gives thus the probability to find values y_{n_i} for mode n. It is at this point that the approach of different physical systems is distinct. For 2D turbulence, W_n and the energy E_n would appear, whereas in classical 3D turbulence, E_n and H_n would appear in expression (3.18).

We have thus, substituting definitions (3.15) and (3.16) in (3.17),

$$P_n\left(y_{n_1},...,y_{n_4}\right) = C_n \exp\left[(-k^2\alpha - k\beta)(y_{n_1}^2 + y_{n_2}^2) + (-k^2\alpha + k\beta)(y_{n_3}^2 + y_{n_4}^2)\right]. \tag{3.19}$$

We define Z_n the integral of P_n,

$$Z_n = \iiiint P_n \mathrm{d}y_{n_1}\mathrm{d}y_{n_2}\mathrm{d}y_{n_3}\mathrm{d}y_{n_4}. \tag{3.20}$$

The average enstrophy per mode is given by

$$\langle W_n\rangle = \sum_{i=1..4}\langle k^2 y_{n_i} y_{n_i}\rangle \tag{3.21}$$

$$= \sum_{i=1..4}\frac{1}{Z_n}\iiiint \left[k^2 P_n y_{n_i} y_{n_i}\right]\mathrm{d}y_{n_1}\mathrm{d}y_{n_2}\mathrm{d}y_{n_3}\mathrm{d}y_{n_4}. \tag{3.22}$$

From Eq. (3.17) and Eq. (3.20) it is observed that we can compute the average directly using

$$-\frac{1}{Z_n}\frac{\partial Z_n}{\partial \alpha} = \langle W_n\rangle, \tag{3.23}$$

and similarly

$$-\frac{1}{Z_n}\frac{\partial Z_n}{\partial \beta} = \langle H_n\rangle. \tag{3.24}$$

The integral (3.20) can be computed to yield,

$$Z_n = \frac{\pi^2}{k^4\alpha^2 - k^2\beta^2}, \tag{3.25}$$

so that we find for the enstrophy and helicity,

$$\langle W_n\rangle = \frac{2\alpha k^2}{\alpha^2 k^2 - \beta^2}, \quad \langle H_n\rangle = \frac{2\beta}{\alpha^2 k^2 - \beta^2}. \tag{3.26}$$

The enstrophy spectrum and helicity spectrum are therefore, due to isotropy,

$$W(k) = \frac{8\pi\alpha k^4}{\alpha^2 k^2 - \beta^2}, \quad H(k) = \frac{8\pi\beta k^2}{\alpha^2 k^2 - \beta^2}. \tag{3.27}$$

so that the kinetic energy spectrum writes

$$E(k) = \frac{8\pi\alpha k^2}{\alpha^2 k^2 - \beta^2}. \tag{3.28}$$

This last expression is the principal theoretical result of the present investigation. An important feature of this expression, in contrast to expression (2.5) derived for classical turbulence, is that in the present case helicity does mainly affect the large scales. Expression (3.28) and its implications will be verified using simulations.

3.3. *Integral relations between the enstrophy, helicity and energy for the equilibrium distributions*

Since the enstrophy and helicity are conserved quantities of the system, the statistical characterization of our system in statistical equilibrium is completely determined by the

values of the enstrophy and helicity,

$$W = \int_{k_{\min}}^{k_{\max}} k^2 E(k) \mathrm{d}k \quad H = \int_{k_{\min}}^{k_{\max}} H(k) \mathrm{d}k \tag{3.29}$$

as soon as we know $k_{\min}$ and $k_{\max}$ and the initial conditions. Indeed, the unknown coefficients α and β in the equilibrium spectra are fully determined by the other parameters. This allows to predict the long-time expected value of the kinetic energy

$$E = \int_{k_{\min}}^{k_{\max}} E(k) \mathrm{d}k, \tag{3.30}$$

as a function of the enstrophy and helicity. Let us illustrate this for the simplest, mirror-symmetric case. For that case we have $\beta = 0$, leading to

$$W = \int_{k_{\min}}^{k_{\max}} 8\pi \frac{k^2}{\alpha} \approx \frac{8\pi}{3} \frac{k_{\max}^3}{\alpha}, \tag{3.31}$$

which allows to express α as a function of W and $k_{\max}$, where we used that $k_{\min} \ll k_{\max}$. Substituting this in the kinetic energy spectrum and integrating yields

$$E \approx 3 \frac{W}{k_{\max}^2}. \tag{3.32}$$

so that we have a prediction for the final value of the kinetic energy as a function of the initial condition for W. When both helicity and enstrophy are nonzero, the computation becomes more tedious, but can still be performed analytically. We introduce the ratio $\gamma = \beta/\alpha$ so that the helicity spectrum writes

$$H(k) = \frac{8\pi\gamma}{\alpha} \frac{k^2}{k^2 - \gamma^2}. \tag{3.33}$$

For this expression to make sense, the minimum wavenumber should verify $k_{\min} > \gamma$. Under this constraint, we can integrate the helicity spectrum to obtain the expression

$$H = \frac{8\pi\gamma}{\alpha} \left(k_{\max} - k_{\min} + \frac{\gamma}{2} \ln \left(\frac{k_{\max}^2 - \gamma^2}{k_{\min}^2 - \gamma^2} \right) \right), \tag{3.34}$$

which relates the helicity to $k_{\max}$, $k_{\min}$, α and β. For the helical cases, the relation between energy and helicity is simply $E = H/\gamma$.

4. Numerical method and initial conditions

Direct numerical simulations (DNS) for the Euler equations without vortex-stretching are performed using a standard pseudo-spectral solver with a third-order Adams-Bashforth time integration scheme. The original code (Delache *et al.* (2014)) is formulated in velocity-formulation and has to be adapted to be able to compute the Euler-equations without vortex-stretching Eq. (1.1). The vortex-stretching is most conveniently removed from the vorticity equation. Using Fourier-representation, the velocity equation is then readily obtained by uncurling the equation (see Bos (2021) for details). Indeed, since for an incompressible vector field we have $\nabla \times \nabla \times \boldsymbol{u} = -\Delta \boldsymbol{u}$, we obtain by taking the curl of Eq. (1.1) the Laplacian of the velocity-equation,

$$\frac{\partial \Delta \boldsymbol{u}}{\partial t} - \nabla \times (\boldsymbol{u} \cdot \nabla \boldsymbol{\omega}) = 0, \tag{4.1}$$

so that for the Fourier-coefficients $\hat{\boldsymbol{u}}$ we can write

$$\frac{\partial \hat{\boldsymbol{u}}}{\partial t} + \frac{\mathrm{i}}{k^2}\boldsymbol{k} \times \mathcal{F}[\boldsymbol{u} \cdot \nabla \boldsymbol{\omega}] = 0, \tag{4.2}$$

where $\mathcal{F}[\bullet]$ indicates the Fourier transform. This formulation conserves by nature incompressibility. Eq. (4.2) is integrated in our code.

Our computational domain is a periodic box in three dimensions with length of side $L = 2\pi$ and a grid of size 128^3. Higher resolutions do not seem necessary in the present case to assess the analytical results.

Aliasing errors are removed using the 2/3 rule, i.e., the maximum wave number is $k_{\max} = [\frac{128}{3}] \times \frac{2\pi}{L} = 43$ where $[\bullet]$ is a rounding operation. The initial energy spectrum is defined as

$$E(k) = C_E\,(k/k_0)^4\, e^{-2(k/k_0)^2} \tag{4.3}$$

with $k_0 = 2.52$ and C_E a constant. The initial complex arguments of velocity in Fourier space are chosen randomly. This method generates initial fields with non-zero helicity. We want to test our predictions for both mirror-symmetric flows and flows with mean-helicity. In order to generate a helicity-free flow it is in principle possible to manipulate the phases of the Fourier modes, but we have used a more intuitive manner by combining two velocity fields.

We generate two velocity fields $\boldsymbol{u}_a$ and $\boldsymbol{u}_b$ with identical energy spectra but different random phases. Then a helicity-free velocity field can be created by a linear combination of these two fields as $\boldsymbol{u}_c = \boldsymbol{u}_a + \lambda \boldsymbol{u}_b$. The constant λ will be determined now. We first introduce the notation

$$h_{ab} \equiv \frac{1}{2}\langle \boldsymbol{u}_a \cdot \boldsymbol{\omega}_b \rangle. \tag{4.4}$$

The mean helicity of field $\boldsymbol{u}_c$ is

$$\begin{aligned} H_c \equiv h_{cc} &= \frac{1}{2}\langle \boldsymbol{u}_c \cdot \boldsymbol{\omega}_c \rangle = \frac{1}{2}\langle (\boldsymbol{u}_a + \lambda \boldsymbol{u}_b) \cdot (\boldsymbol{\omega}_a + \lambda \boldsymbol{\omega}_b) \rangle \\ &= \frac{1}{2}(h_{aa} + \lambda(h_{ab} + h_{ba}) + \lambda^2 h_{bb}). \end{aligned} \tag{4.5}$$

Since $h_{aa}, h_{bb}, h_{ab}, h_{ba}$ can all be computed directly, the condition $H_c = 0$ yields a quadratic equation for λ [i.e. Eq. (4.5)=0], which can be solved exactly to determine λ. This procedure allows to generate a zero-helicity initial condition with prescribed kinetic energy spectrum. Due to rounding errors the helicity of the resulting initial condition is order 10^{-4}, which is sufficiently close to zero for our purposes.

5. Numerical investigation of the equilibrium states

In this section we will assess numerically the conservation of enstrophy and helicity. Subsequently we will check our predictions from statistical mechanics and show visualizations of the equilibrium state.

5.1. *Conservation of enstrophy and helicity during relaxation*

In Fig. 2 we show the time evolution of enstrophy, helicity and kinetic energy. Note that the initial energy E_0 is unity. Time is normalized by a characteristic time scale $\tau = 1/\sqrt{E_0 k_{min}^2}$. For the case of mirror-symmetric truncated Euler-turbulence without vortex-stretching, a clear conservation of enstrophy is observed, whereas the kinetic energy decays. Helicity remains negligible throughout the simulation. The prediction of the kinetic energy, discussed

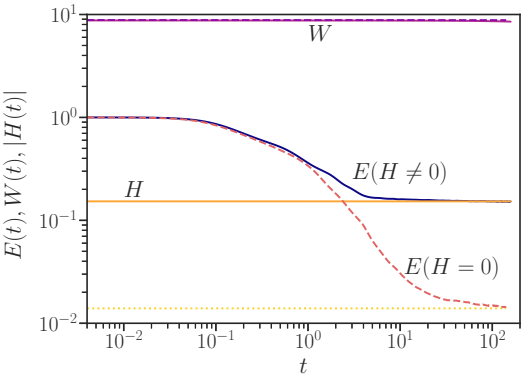

Figure 2: Time evolution of energy, enstrophy and helicity for the inviscid, force-free, 3D, no vortex-stretching turbulence. (solid lines: helical case; dashed lines: mirror-symmetric case; dotted line: the analytical prediction of the kinetic energy for the mirror-symmetric case.)

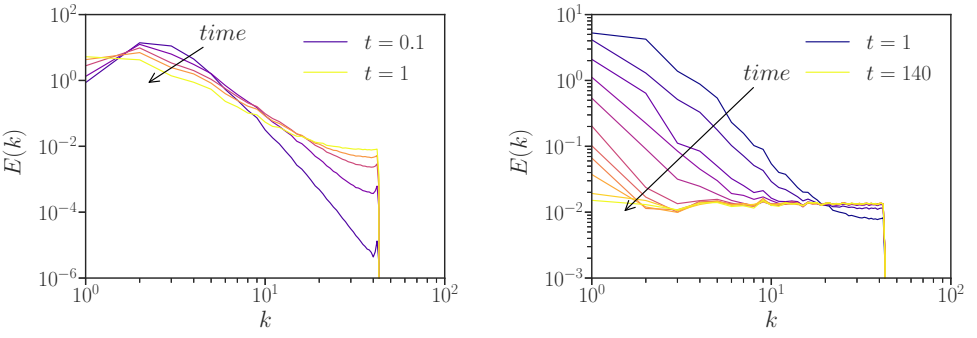

(a) (b)

Figure 3: Inviscid relaxation for helicity-free turbulence. (a) Short time evolution, showing the kinetic energy spectra at t = 0.1; 0.2; 0.4; 0.6; 1. (b) Long time evolution, showing the spectra at t = 1; 2; 4; 6; 10; 20; 40; 60; 100; 120; 140.

in Sec. 3.3 is represented by a dotted line. It is observed that the expected steady state is reached for the kinetic energy. This steady state is the predicted equilibrium state, where the Fourier-modes all contain, on average, the same amount of enstrophy.

In Fig. 2 the same results are also plotted for the helical case. It is observed, that as shown in our proof (Sec. 3.1), helicity is conserved by the system. As mentioned in Sec. 3.3, the prediction of the final kinetic energy in the helical case is $E = H/\gamma$. After calculation, we have $\gamma = -0.9989 \approx -1$ in our simulation. This corresponds to the observation that the kinetic energy tends to the absolute value of the helicity. This tendency is not a coincidence, but reflects the condensation of energy into a helical flow-structure at scales with wavenumber $k = 1$, as will be shown next. It is also shown that the presence of helicity allows the flow to retain more kinetic energy in the system than the mirror-symmetric case does. Indeed, whereas without helicity, the energy drops to less than 2% of its initial value, in the helical case, this value is approximately 15%.

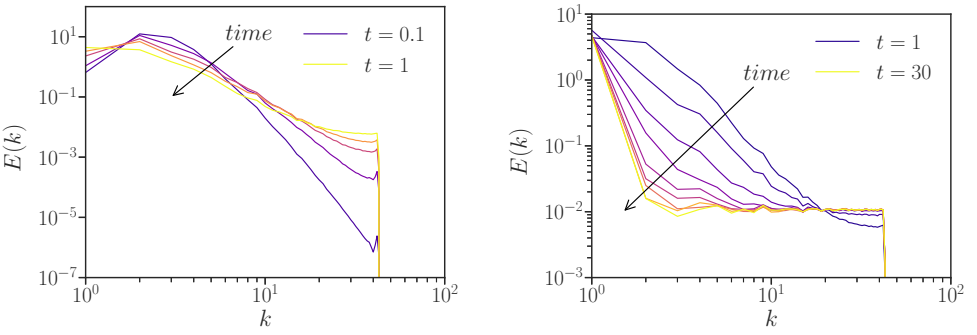

(a) (b)

Figure 4: Inviscid relaxation for helical turbulence. (a) Short time evolution, showing the kinetic energy spectra at t = 0.1; 0.2; 0.4; 0.6; 1. (b) Long time evolution, showing the spectra at t = 1; 2; 4; 6; 8; 10; 14; 16; 18; 30.

To further investigate the dynamics of the truncated system, we show in Fig. 3(a,b) the evolution of the kinetic energy spectra towards the equilibrium state. It is observed that enstrophy accumulates rapidly in the largest spatial frequencies, in a similar manner as energy accumulates in classical truncated Euler dynamics (Cichowlas *et al.* 2005; Bos & Bertoglio 2006). This evolution was correctly predicted and explained in Bos (2021).

The dynamics of the helical case (Fig. 4(a,b)) is quite similar, except for the persistent energy in the smallest wavenumbers. This is anticipated by the statistical-mechanics predictions in Sec. 3 and we will focus on them now.

5.2. *Comparison with predicted shapes*

In Fig. 5 we compare the spectra associated to the relaxed state, obtained from the numerical simulations, to the predictions (3.27 and 3.28) for the spectra. An excellent agreement is observed. Fig. 5(a) shows the mirror-symmetric case, where a flat energy spectrum, associated with equidistributed enstrophy is obtained. We do not show the enstrophy spectrum which is simply obtained by the energy spectrum multiplied by k^2.

The most flagrant difference between the mirror-symmetric and helical cases is the accumulation of helicity near the infra-red cut-off. In Fig. 5(b) we observe this for the energy spectrum, and the same feature is observed for the enstrophy and helicity spectrum in Fig. 5(c) and Fig. 5(d). The amount of energy in this large-scale feature is quite important. Indeed, the $k = 1$ mode contains 87% of the total energy. We will now focus on this energetic, helical mode.

5.3. *Visualization of the final state*

An instantaneous visualization of the y-component of the velocity for the final state is visualized in Fig. 6. It shows that our 3D, inviscid, no vortex-stretching system relaxes to a large-scale structure. This could be suspected from the energy spectrum, and it is illustrated in the visualizations. Since almost all energy and all helicity is contained in the $k = 1$ mode, a plausible three-dimensional structure is the Arnold-Beltrami-Childress, or ABC, flow. A physical explanation for this, in the light of the statistical mechanics description used here, is that adding the additional constraint of helicity conservation will change the energy and therefore the enstrophy distribution. This will necessarily lead to a decrease of the entropy of the system, since the highest entropy corresponds to enstrophy equipartition.

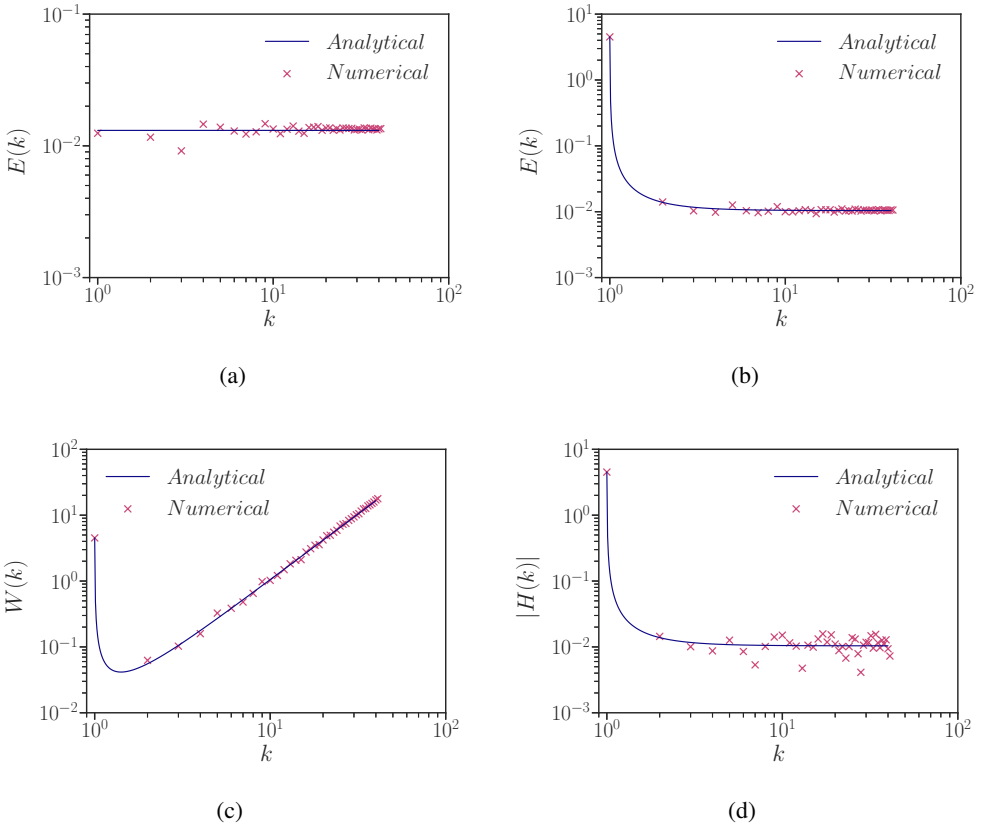

Figure 5: Analytical spectra associated with the absolute equilibrium state and numerical spectra. (a) Energy spectrum of the helicity-free case at $t = 140$. (b-d) Helical case at $t = 30$. (b) Energy spectrum. (c) Enstrophy spectrum. (d) Absolute value of helicity spectrum.

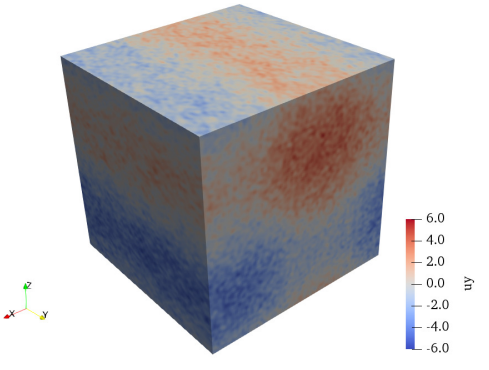

Figure 6: Visualizations of the truncated inviscid system without vortex-stretching, obtained from pseudo-spectral computations. Velocity in the y-direction (u_y).

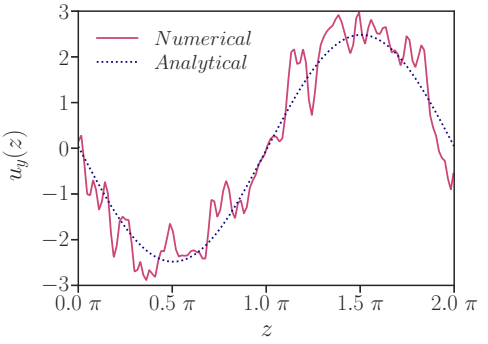

Figure 7: Visualization of flow and verification of ABC flow proprieties. Analytical and numerical results of $u_y(z)$ along the line ($x = 0.66L$, $y = 0.5L$).

The minimum change in entropy corresponds to a modification of the largest scales of the system. Maximizing the helicity in the largest scales of the system is therefore the most probable reaction of the system. Maximum helicity corresponds to alignment of velocity and vorticity, and thus to an ABC flow. In the following, we verify that the $k = 1$ contribution of the equilibrium state corresponds to such a flow.

The definition of an ABC flow with typical size L is

$$\begin{aligned} u_x &= A \sin \tilde{z} + C \cos \tilde{y}, \\ u_y &= B \sin \tilde{x} + A \cos \tilde{z}, \\ u_z &= C \sin \tilde{y} + B \cos \tilde{x}, \end{aligned} \tag{5.1}$$

where $\tilde{x}_i = \pm 2\pi x_i / L + \phi_i$. The $\pm$ sign determines the sign of helicity. Simple algebra shows that the parameters A, B, C satisfy the relations

$$\begin{aligned} A^2 &= \left\langle u_x^2 \right\rangle + \left\langle u_y^2 \right\rangle - \left\langle u_z^2 \right\rangle, \\ B^2 &= \left\langle u_y^2 \right\rangle + \left\langle u_z^2 \right\rangle - \left\langle u_x^2 \right\rangle, \\ C^2 &= \left\langle u_z^2 \right\rangle + \left\langle u_x^2 \right\rangle - \left\langle u_y^2 \right\rangle. \end{aligned} \tag{5.2}$$

We measure during equilibrium $\left\langle u_x^2 \right\rangle = 3.7963$, $\left\langle u_y^2 \right\rangle = 4.2210$ and $\left\langle u_z^2 \right\rangle = 1.8600$. These figures yield $|A| = 2.4814$, $|B| = 1.5115$ and $|C| = 1.1980$. Averaging the three relations (5.1) for fixed positions x, y, z allows also to determine the phases ϕ_i. Doing so for our simulation, we find $\widetilde{x} = -2\pi x/L - 0.66\pi$, $\widetilde{y} = -2\pi y/L - 0.25\pi$, $\widetilde{z} = -2\pi z/L - 0.495\pi$ with $A > 0$, $B > 0$, $C > 0$.

In Fig. 7 we compare the resulting ABC-flow prediction to the results of the simulation for an arbitrary cut through the domain along the z-direction, plotting the y-velocity. The large-scale flow is indeed consistent with an ABC flow pattern. Superposed upon this large-scale pattern, we observe random fluctuations with a larger spatial frequency, consistent with the spectra we showed in the previous section. All other velocity-components in all other directions (not shown) confirm this behavior of an ABC structure accompanied by large-frequency noise.

6. Conclusions

The main insight obtained in the present investigation can be summarized by the spectra in Fig. 5. These figures illustrate the statistical equilibrium states of a truncated set of Fourier-modes, governed by the Euler-equations without vortex-stretching. The kinetic energy spectrum is flat for large wavenumbers, as was predicted in Bos (2021). However, the largest scales allowed by the system are strongly affected if the initial conditions contain helicity.

In the absence of helicity, the final state corresponds to a thermal equilibrium of Fourier modes over which enstrophy is evenly distributed, on average. As soon as helicity is present, the helicity allows a condensation of energy in the largest scales of the system. The flow-structure associated with this is an Arnold-Beltrami-Childress flow and the energy of this structure is directly determined by the amount of helicity in the system. It is shown in the simulations carried out here that the initial amount of normalized helicity does not need to be very large to have a large influence on the final state. Indeed, since the helicity is conserved, the decrease of the kinetic energy (and constant enstrophy) leads to an increase of its normalized value at the end.

The tendency of the largest scales of the inviscid system to absorb the helicity does have implications for the cascade directions in a forced-dissipative system. Indeed, in turbulence without vortex stretching, enstrophy is preferentially transfered to the large wavenumbers (Bos 2021). In order to approach the equilibrium state, helicity will presumably show a tendency to be transferred to small wavenumbers. The verification of such a novel dual cascade scenario will be left for further research.

As a perspective we also plan to consider how these ideas carry over to two-dimensional three-component flows. Indeed, in such flows vortex-stetching is also suppressed and thereby helicity conserved by the nonlinearity. Whether such systems similarly relax to a helical large-scale dynamics is a question which could have interesting geophysical applications. An interesting first result pointing towards the importance of large-scale helical motion in such systems can be found in Agoua *et al.* (2021), where a forced 2D3C flow is shown to generate large-scale helical motion.

Acknowledgments

We thank Antoine Venaille for pointing us to useful references on statistical mechanics applied to turbulence. All simulations were carried out using the facilities of the PMCS2I (École Centrale de Lyon). We gratefully thank Laurent Pouilloux and Wesley Agoua for helpful advice. Financial support of the Chinese Scholarship Council (CSC) and ANR project CM2E is acknowledged.

Declaration of interests

The authors report no conflict of interest.

REFERENCES

Agoua, W., Favier, B., Delache, A., Briard, A. & Bos, W.J.T. 2021 Spontaneous generation and reversal of helicity in anisotropic turbulence. *Physical Review E* **103** (6), L061101.

Alexakis, A. 2017 Helically decomposed turbulence. *Journal of Fluid Mechanics* **812**, 752.

Alexakis, A. & Brachet, M.-E. 2019 On the thermal equilibrium state of large-scale flows. *Journal of Fluid Mechanics* **872**, 594–625.

André, J.C. & Lesieur, M. 1977 Influence of helicity on the evolution of isotropic turbulence at high Reynolds number. *J. Fluid Mech* **81**, 187.

Batchelor, G.K. 1969 Computation of the energy spectrum in homogeneous two-dimensional turbulence. *Phys. Fluids* **12**, II–233.

Biferale, L., Buzzicotti, M. & Linkmann, M. 2017 From two-dimensional to three-dimensional turbulence through two-dimensional three-component flows. *Physics of Fluids* **29** (11), 111101.

Biferale, L., Musacchio, S. & Toschi, F. 2012 Inverse energy cascade in three-dimensional isotropic turbulence. *Physical review letters* **108** (16), 164501.

Borue, V. & Orszag, S.A. 1997 Spectra in helical three-dimensional homogeneous isotropic turbulence. *Physical Review E* **55** (6), 7005.

Bos, W.J.T. 2021 Three-dimensional turbulence without vortex stretching. *Journal of Fluid Mechanics* **915**, A121.

Bos, W.J.T. & Bertoglio, J.P. 2006 Dynamics of spectrally truncated inviscid turbulence. *Phys. Fluids* **18**, 071701.

Bouchet, F. & Venaille, A. 2012 Statistical mechanics of two-dimensional and geophysical flows. *Physics Reports* **515**, 227.

Buaria, D., Pumir, A. & Bodenschatz, E. 2020 Self-attenuation of extreme events in navier–stokes turbulence. *Nature communications* **11** (1), 1–7.

Cambon, C. & Jacquin, L. 1989 Spectral approach to non-isotropic turbulence subjected to rotation. *J. Fluid Mech.* **202**, 295–317.

Carbone, M. & Bragg, A.D. 2020 Is vortex stretching the main cause of the turbulent energy cascade? *Journal of Fluid Mechanics* **883**.

Cichowlas, C., Bonaïti, P., Debbasch, F. & Brachet, M. 2005 Effective dissipation and turbulence in spectrally truncated Euler flows. *Phys. Rev. Lett.* **95**, 264502.

Constantin, P. 2007 On the euler equations of incompressible fluids. *Bulletin of the American Mathematical Society* **44** (4), 603–621.

Davidson, P.A. 2013 *Turbulence in rotating, stratified and electrically conducting fluids*. Cambridge University Press.

Delache, A., Cambon, C. & Godeferd, F. 2014 Scale by scale anisotropy in freely decaying rotating turbulence. *Phys. Fluids* **26** (2), 025104.

Eyink, G.L. & Spohn, H. 1993 Negative-temperature states and large-scale, long-lived vortices in two-dimensional turbulence. *Journal of statistical physics* **70** (3), 833–886.

Frisch, U. 1995 *Turbulence, the legacy of A.N. Kolmogorov*. Cambridge University Press.

Frisch, U., Pomyalov, A., Procaccia, I. & Ray, S.S. 2012 Turbulence in noninteger dimensions by fractal fourier decimation. *Physical review letters* **108** (7), 074501.

Frisch, U., Pouquet, A., Léorat, J. & Mazure, A. 1975 Possibility of an inverse cascade of magnetic helicity in magnetohydrodynamic turbulence. *Journal of Fluid Mechanics* **68** (4), 769–778.

Fyfe, D. & Montgomery, D. 1976 High-beta turbulence in two-dimensional magnetohydrodynamics. *Journal of Plasma Physics* **16** (2), 181–191.

Hou, T.Y. & Li, R. 2006 Dynamic depletion of vortex stretching and non-blowup of the 3-d incompressible euler equations. *Journal of Nonlinear Science* **16** (6), 639–664.

Johnson, P.L. 2020 Energy transfer from large to small scales in turbulence by multiscale nonlinear strain and vorticity interactions. *Physical review letters* **124** (10), 104501.

van Kan, A., Alexakis, A. & Brachet, M. 2021 Geometric microcanonical theory of two-dimensional truncated euler flows. *arXiv preprint arXiv:2104.11282* .

Kerr, R.M. 1993 Evidence for a singularity of the three-dimensional, incompressible euler equations. *Physics of Fluids A: Fluid Dynamics* **5** (7), 1725–1746.

Kolmogorov, A.N. 1941 The local structure of turbulence in incompressible viscous fluid for very large Reynolds numbers. *Dokl. Akad. Nauk. SSSR* **30**, 301.

Kraichnan, R.H. 1967 Intermittency in the very small scales of turbulence. *Phys. Fluids* **10**, 2080.

Kraichnan, R.H. 1971 An almost-Markovian Galilean-invariant turbulence model. *J. Fluid Mech.* **47**, 513.

Kraichnan, R.H. 1973 Helical turbulence and absolute equilibrium. *J. Fluid Mech.* **59**, 745.

Kraichnan, R.H. & Montgomery, D. 1980 Two-dimensional turbulence. *Reports on Progress in Physics* **43** (5), 547.

Lee, T.D. 1952 On some statistical properties of hydrodynamical and magnetohydrodynamical fields. *Q. Appl. Math* **10**, 69.

Leith, C.E. 1968 Diffusion approximation for two-dimensional turbulence. *Phys. Fluids* **11**, 671.

Leprovost, N., Dubrulle, B. & Chavanis, P.-H. 2006 Dynamics and thermodynamics of axisymmetric flows: Theory. *Physical Review E* **73**, 046308.

Lesieur, M. 1990 *Turbulence in fluids*. Kluwer Dordrecht.

Lundgren, T.S. & Pointin, Y.B. 1977 Statistical mechanics of two-dimensional vortices. *J. Stat. Phys.* **17** (5), 323–355.

Miller, J. 1990 Statistical mechanics of Euler equations in two dimensions. *Phys. Rev. Lett.* **65**, 2137–2140.

Moffatt, H.K. 1969 The degree of knottedness of tangled vortex lines. *Journal of Fluid Mechanics* **35** (1), 117–129.

Mohseni, K. 2001 Statistical equilibrium theory for axisymmetric flows: Kelvin's variational principle and an explanation for the vortex ring pinch-off process. *Phys. Fluids* **13** (7), 1924–1931.

Montgomery, D.C. & Joyce, G. 1974 Statistical mechanics of "negative temperature" states. *Phys. Fluids* **17**, 1139.

Moreau, J.J. 1961 Constantes d'un îlot tourbillonnaire en fluide parfait barotrope. *Comptes rendus hebdomadaires des séances de l'Académie des sciences* **252**, 2810–2812.

Naso, A., Monchaux, R., Chavanis, P.H. & Dubrulle, B. 2010 Statistical mechanics of beltrami flows in axisymmetric geometry: Theory reexamined. *Phys. Rev. E* **81**, 066318.

Onsager, L. 1949 Statistical hydrodynamics. *Il Nuovo Cimento* **6**, 279.

Robert, R. & Sommeria, J. 1991 Statistical equilibrium states for two-dimensional flows. *J. Fluid Mech.* **229**, 291.

Sagaut, P. & Cambon, C. 2008 *Homogeneous Turbulence Dynamics*. Cambridge University Press.

Salmon, R. 1998 *Lectures on geophysical fluid dynamics*. Oxford University Press.

Salmon, R. 2013 Coupled systems of two-dimensional turbulence. *Journal of Fluid Mechanics* **732**.

Servidio, S., Matthaeus, W.H. & Dmitruk, P. 2008 Depression of nonlinearity in decaying isotropic mhd turbulence. *Phys. Rev. Lett.* **100**, 095005.

Shukla, V., Fauve, S. & Brachet, M. 2016 Statistical theory of reversals in two-dimensional confined turbulent flows. *Physical Review E* **94** (6), 061101.

Thalabard, S. 2013 Contributions to the statistical mechanics of ideal two and a half dimensional flows. PhD thesis, Université Paris Sud-Paris XI.

Venaille, A., Gostiaux, L. & Sommeria, J. 2017 A statistical mechanics approach to mixing in stratified fluids. *Journal of Fluid Mechanics* **810**, 554.

Waleffe, F. 1992 The nature of triad interactions in homogeneous turbulence. *Physics of Fluids A: Fluid Dynamics* **4** (2), 350–363.

Zhu, J.-Z. & Hammett, G.W. 2010 Gyrokinetic statistical absolute equilibrium and turbulence. *Physics of Plasmas* **17** (12), 122307.